

# Two-Focus Fluorescence Correlation Spectroscopy: A New Tool for Accurate and Absolute Diffusion Measurements

Thomas Dertinger,<sup>[a]</sup> Victor Pacheco,<sup>[b]</sup> Iris von der Hocht,<sup>[a]</sup> Rudolf Hartmann,<sup>[b]</sup> Ingo Gregor,<sup>[a]</sup> and Jörg Enderlein<sup>\*[a]</sup>

*We present a new method to measure absolute diffusion coefficients at nanomolar concentrations with high precision. Based on a modified fluorescence correlation spectroscopy (FCS)-setup, this method is improved by introducing an external ruler for measuring the diffusion time by generating two laterally shifted and overlapping laser foci at a fixed and known distance. Data fitting is facilitated by a new two-parameter model to describe the molecule detection function (MDF). We present a recorded MDF and show the excellent agreement with the fitting model.*

*We measure the diffusion coefficient of the red fluorescent dye Atto655 under various conditions and compare these values with a value achieved by gradient pulsed field NMR (GPF NMR). From these measurements we conclude, that the new measurement scheme is robust against optical and photophysical artefacts which are inherent to standard FCS. With two-focus-FCS, the diffusion coefficient of  $4.26 \times 10^{-6} \text{ cm}^2 \text{ s}^{-1}$  for Atto655 in water at  $25^\circ \text{C}$  compares well with the GPF NMR value of  $4.28 \times 10^{-6} \text{ cm}^2 \text{ s}^{-1}$ .*

## 1. Introduction

Thermally induced translational diffusion is one of the fundamental properties exhibited by molecules within a solution. Via the Stokes-Einstein relation it is directly coupled with the hydrodynamic radius of the molecules.<sup>[1]</sup> Any change in that radius will change the associated diffusion coefficient of the molecules. Such changes occur to most biomolecules—in particular proteins, RNA and DNA—when interacting with their environment (e.g. binding of ions or other biomolecules) or performing biologically important functions (e.g. enzymatic catalysis) or reacting to changes in environmental parameters such as pH, temperature, or chemical composition (e.g. protein unfolding). Therefore, the ability to precisely measure diffusion coefficients has a large range of potential applications, for monitoring for example, conformational changes in proteins upon ion binding or unfolding. However, many biologically relevant conformational changes are connected with rather small changes in hydrodynamic radius on the order of Ångströms (see for example, ref. [2]). To monitor these small changes, it is necessary to measure the diffusion coefficient with an accuracy of better than a few percent. Standard methods for diffusion coefficient measurements achieving this accuracy are dynamic light scattering (DLS),<sup>[3]</sup> pulsed field gradient NMR,<sup>[4]</sup> size exclusion electrophoresis,<sup>[5]</sup> or analytical ultracentrifugation.<sup>[6]</sup> However, all these methods operate at rather high sample concentrations, far away from the limit of infinite dilution. For obtaining the correct infinite-dilution limit and thus a correct estimate of the hydrodynamic radius, one has often to measure at different concentrations and to extrapolate the concentration/diffusion coefficient curve towards zero concentration (see for example, ref. [7]). Another problem is that proteins are often

prone to aggregation<sup>[8]</sup> at the concentrations needed for obtaining sufficient data quality.

Several decades ago, Magde, Elson and Webb invented an ingenious alternative method for measuring diffusion coefficients of fluorescent molecules: fluorescence correlation spectroscopy (FCS).<sup>[9–11]</sup> In FCS, the fluorescence fluctuations detected out of a very small detection volume (usually on the order of one femtoliter or less) are recorded, and the resulting signal is autocorrelated, yielding the second order or autocorrelation function (ACF) of the fluctuating signal. If the average number of molecules within the detection volume is sufficiently small, the fluctuations are dominated by the random diffusion of the fluorescent molecules out of that volume, and the ACF shows a prominent decay which is characterized by the diffusion coefficient of the molecules. This method works best if, on average, about one molecule is present within the detection volume. Thus, it is optimally suited for working at nanomolar concentrations. Consequently, values for the diffusion coefficient obtained by FCS are indistinguishable from their infinite dilution value, and the method circumvents most aggregation

[a] T. Dertinger, I. von der Hocht, Dr. I. Gregor, Dr. J. Enderlein  
Institut für Biologische Informationsverarbeitung 1  
Forschungszentrum Jülich  
52425 Jülich (Germany)  
Fax: (+49) 2461-618069  
E-mail: j.enderlein@fz-juelich.de

[b] Dr. V. Pacheco, Dr. R. Hartmann  
Institut für Biologische Informationsverarbeitung 2  
Forschungszentrum Jülich  
52425 Jülich (Germany)

problems. Another significant advantage of FCS is its relative technical simplicity, at least when compared to such methods as NMR.

Over the recent decades, FCS has found manifold applications in biology and chemistry, see for example, refs. [12, 13]. However, as the method became widely available and popular, its limitations became also visible. As stated above FCS measures how quickly, on average, molecules diffuse out of the detection volume. For calculating the diffusion coefficient, one has to have precise knowledge about shape and size of this volume, or more precisely, the molecule detection function (MDF) that describes the position-dependent probability to excite and detect a fluorescence photon from a molecule at a given position within the sample. The standard assumption is that the MDF can be approximated by a three-dimensional Gaussian profile, and that the Gaussian half axes can be determined by measuring a reference sample with known diffusion coefficient.<sup>[14]</sup> However, it is known for many years that the assumption of a three-dimensional Gaussian MDF is rather inaccurate.<sup>[15, 16]</sup> Over the last years, an increasing number of publications has shown the sensitivity of FCS measurements for even smallest changes in experimental conditions such as cover slide thickness variation, refractive index mismatch, or laser beam characteristics, see for example, refs. [17, 18]. One of the most disturbing observations was the dependence of a measured ACF on excitation intensity due to optical saturation of fluorescence which occurs even at very low total excitation power.<sup>[19–21]</sup> This makes even comparative measurements problematic, because the photophysics and thus optical saturation properties of fluorescence labels often change when they are chemically bound to a target molecule.

Several authors have proposed and evaluated modified concepts of FCS by using optical excitation and/or detection schemes to achieve better definition and control of the MDF. In particular, one tried to introduce an *external ruler* into the measurement, which is absent in standard FCS. Among these attempts where FCS in front of dielectric mirrors,<sup>[22]</sup> standing wave FCS,<sup>[23]</sup> total internal reflectance fluorescence (TIRF)-FCS,<sup>[24]</sup> or spatial correlation FCS between two detection volumes generated by detecting fluorescence through two laterally shifted pinholes.<sup>[25]</sup> The external ruler was provided either by the known modulation length of a standing light wave, or the estimated distance between the detection volumes. However, all the proposed methods suffer from the problem that for a precise quantification of the diffusion coefficient one still needs precise knowledge of the overall shape of the MDF. For example, when focusing a laser onto a dielectric mirror for generating an interference excitation intensity pattern with well-defined pattern periodicity along the optical axis, the overall shape of the MDF and thus the resulting ACF are still sensitively dependent on the precise relative position of laser focus and the mirror, making a quantitative determination of the diffusion coefficient still cumbersome. The same argument applied for standing wave FCS, where one has to perfectly align the foci of two counter-propagating laser beams. More seriously, in both methods, the fast decay of the ACF introduced by the standing excitation wave pattern is usually on

the same timescale (few  $\mu\text{s}$ ) as fast photophysical processes such as triplet-state or light-induced *cis-trans* isomerization making a clear distinction between diffusion-induced and photophysics-induced ACF behavior very difficult. In TIRF-FCS, the MDF depends not only on the evanescent wave excitation, but also on the peculiarities of fluorescence detection close to an interface,<sup>[26]</sup> leading to a significant deviation of the dependence of the MDF along the optical axis from the simple exponential (which is mostly ignored in many publications concerned with TIRF). Moreover, one will generally prefer a measurement technique that can operate far from any interface. Finally, spatial correlation FCS between two detection volumes generated by detecting fluorescence through two laterally shifted pinholes leads to very complicated, asymmetric MDFs, making again quantitative determination of diffusion coefficients rather complicated. Also, it is difficult to assure an exact known and unchangeable lateral distance between the detection volumes with nanometer precision, which requires the perfect alignment of two confocal apertures in the two detection channels.

In the present paper we propose a new and straightforward scheme for a modified FCS technique, termed 2-focus FCS or 2fFCS, using two overlapping foci and globally evaluating the auto-correlation of each focus together with the cross-correlation function between the foci. FCS measurement set-ups with two foci in two detection regions have been already described and used in the past.<sup>[27–29]</sup> In all these publications, the foci were not<sup>[27, 28]</sup> or only marginally<sup>[29]</sup> overlapping, and the set-ups were used for measuring *flow velocities* of fluorescent tracers in moving liquids. Non-overlapping foci with rather large distances ( $\mu\text{m}$  range) are perfectly suited for flow velocity measurements but rather unsuitable for diffusion measurements in non-moving liquids. This is caused by the fact that for purely diffusing molecules the amplitude of the cross-correlation between two foci decays exponentially with the square of the focus distance. Thus, to achieve a reasonably low measurement time one has to work with a large focus overlap that is, small distance between both foci. Recently, Ries and Schwille<sup>[30]</sup> introduced a new method using two far-distant but *scanned* foci and a clever temporal alignment of measured fluorescence intensities for realizing a two-focus cross-correlation measurement of slow diffusion in membranes. This approach comes close to the idea presented here although, due to the slowness of mechanical scanning, their set-up cannot measure fast diffusion in solution. All the mentioned two-focus set-ups are based on focusing two laser beams into the sample by means of mirrors and mechanical actuators. The error of diffusion coefficient determination by using the cross-correlation between two foci depends quadratically on the error with which the distance between the foci is known. For example, for an interfocal-distance of 500 nm one has to know the distance within 10 nm accuracy when aiming for an accuracy of the diffusion coefficient measurement of 4%. Although one may be able to measure that distance with required accuracy, standard mechanical adjustments are always prone to drifting and will not be able to keep this distance with nanometer accuracy over long times. Thus, a purely optical genera-

tion of two foci with no moving parts is an essential and crucial element of our 2f-FCS method.

The 2f-FCS method which is proposed and tested in the present paper satisfies two essential requirements: 1) it introduces an external ruler into the measurement by generating two overlapping laser foci of precisely known and fixed distance, 2) it generates the two foci and corresponding detection regions in such a way that the corresponding MDFs are sufficiently well described by a simple two-parameter model yielding accurate diffusion coefficients when applied to 2fFCS data analysis. Both these properties enable us to measure absolute values of the diffusion coefficient with an accuracy of a few percent. Moreover, as is demonstrated experimentally, the new technique is robust against refractive index mismatch and optical saturation effects, which are troublesome in standard FCS measurements.

## Materials and Methods

**Chemicals:** Red fluorescent beads (PS-Speck Microscope Point Source Kit P7220) were purchased by Invitrogen GmbH (Karlsruhe, Germany). Guanidine hydrochloride (>99%, GdHCl) was purchased from Sigma-Aldrich Chemikalien GmbH (Munich, Germany). Atto655 in the form of carboxylic acid and as NHS-ester were purchased from Atto-Tec GmbH (Siegen, Germany). Deuterized  $[D_4]MeOH$  (99.8 atom%) was purchased from Sigma-Aldrich Chemikalien GmbH (Munich, Germany). DOPC and DOPE-Biotin was purchased from Avanti Polar Lipids (Alabaster, AL, USA). DOPE was purchased from Sigma (St. Louis, MO, USA). Other chemicals (methanol, chloroform, glucose) were purchased from Sigma, Fluka (St. Gallen, Switzerland) or kmf Laborchemie Handels GmbH (Lohmar, Germany). Neutravidin was purchased from Pierce Biotechnology Inc. (Rockford, IL, USA). ITO-coated cover slides were purchased from SPI Supplies (West Chester, PA, USA).

**GdHCl Solutions:** Atto655 carboxylic acid was diluted in bi-distilled water. A 6.63 M stock solution of GdHCl in water was prepared. By diluting this stock, solutions with lower GdHCl concentrations were made. Concentration of the dilutions was checked by measuring the refractive indices.

**Labelling of DOPE with Atto655-NHS-Ester:** 1.14  $\mu\text{mol}$  DOPE, 1.14  $\mu\text{mol}$  triethylamine and 1.6  $\mu\text{mol}$  Atto655-NHS-ester were dissolved in 60  $\mu\text{L}$  anhydrous methanol and incubated for 90 min at room temperature. Reaction progress was followed by thin layer chromatography using silica gel 60-F<sub>254</sub> plates (Merck, Darmstadt, Germany). The plates were developed with a 60:25:4 (v/v) mixture of chloroform:methanol:water. Atto655-DOPE was purified by chromatography on a silica gel column (eluent: chloroform:methanol:water 60:25:4 (v/v)). The presence of Atto655-DOPE in each fraction was monitored by thin layer chromatography. The solvent was removed and Atto655-DOPE was dissolved in anhydrous methanol and stored at  $-20^\circ\text{C}$  under a nitrogen atmosphere until use.

**Preparation of Giant Unilamellar Vesicles:** Giant unilamellar vesicles were prepared using the electroformation method introduced by Angelova and Dimitrov.<sup>[31]</sup> Solutions of lipids in chloroform were handled in glassware only and stored at  $-20^\circ\text{C}$  under nitrogen atmosphere. A mixture of labelled and unlabelled lipids (labelling ratio 1:400 000) containing 0.1 mol% biotinylated lipids in chloroform was distributed evenly on one ITO-coated glass slide. The solvent was evaporated under reduced pressure. 4–5  $\mu\text{g cm}^{-2}$  remains on the glass slide. A second ITO-coated glass slide was incubated

with a neutravidin (0.1  $\text{mg mL}^{-1}$ ) solution for 15 min to build a self-assembled protein layer.<sup>[32]</sup> The electroformation cell was assembled by placing a tailored 1 mm thick soft silicone seal between these cover slides which was filled with glucose solution. An electric field (15  $\text{V cm}^{-1}$ , 15 Hz) was applied for 2 h. After formation giant vesicles were immobilised at the neutravidin-coated glass by binding of the biotinylated lipids to neutravidin.

**Pulsed-Field Gradient NMR Spectroscopy:** We performed NMR measurements in deuterated  $[D_4]MeOH$  solutions of Atto655 at three different concentrations: 3.4 mM, 1.1 mM and 0.4 mM. NMR measurements were made with Variant INOVA 600 MHz spectrometer operating at the  $^1\text{H}$  frequency of 599.644 MHz. Self-diffusion coefficient measurements were performed applying the BPP-LED sequence.<sup>[33–39]</sup> The DOSY spectra were acquired at  $25^\circ\text{C}$ . We used a thermostat L900 from Variant with temperature accuracy better than  $\pm 0.05\%$ . The data were collected with no spinning. The self-diffusion coefficients were obtained in the following way. We calibrated our gradient using the  $D$ -values previously obtained by NMR at  $25^\circ\text{C}$  with a methanol  $d_4$  sample,<sup>[40]</sup> namely for  $\text{CD}_3\text{OH}$  ( $D = 2.22 \times 10^{-9} \text{ m}^2 \text{ s}^{-1}$ ) and for  $\text{CHD}_2\text{OD}$  ( $D = 2.18 \times 10^{-9} \text{ m}^2 \text{ s}^{-1}$ ). The gradient strength was logarithmically incremented in 15 steps from 14.52  $\text{G cm}^{-1}$  up to 56.22  $\text{G cm}^{-1}$ . The following experimental settings were used: diffusion time,  $\Delta$  was 40 ms, gradient duration,  $\delta$  was 800  $\mu\text{s}$ , the longitudinal eddy current delay was 20 ms, acquisition time was 3 s. Details of the apparatus and procedure are given elsewhere.<sup>[41–44]</sup> The reported self-diffusion coefficient is averaged over at least 10 measurements which agree to within  $\pm 0.5\%$  and the overall accuracy of the data is estimated to be better than  $\pm 4\%$ .

**2fFCS Measurement Setup:** The 2fFCS setup is based on a standard confocal epi-fluorescence microscope as described in detail in ref. [45] and schematically shown in Figure 1. However, instead of using a single excitation laser, light from two identical, linearly polarized pulsed diode lasers at 640 nm wavelength (LDH-P-635, PicoQuant, Berlin, Germany) are combined by a polarizing beam splitter (Narrow Band Polarizing Beamsplitter Cube 633, Ealing Catalogue, St. Asaph, UK). The laser pulses have 50 ps pulse duration, and both lasers are pulsed *alternately* with an overall repetition rate of 40 MHz (pulsed interleaved excitation or PIE.<sup>[46]</sup> Alternate pulsing is accomplished by special laser driver electronics (PDL 808 "Sepia", PicoQuant, Berlin, Germany). Both beams are then coupled into a polarization maintaining single mode fiber. At the output, the light is again collimated. Thus, the combined light consists of a train of laser pulses with alternating orthogonal polarization. The beam is then reflected by a dichroic mirror (Q 660 LP, Chroma Technology, Rockingham, VT, USA) towards the microscope's water-immersion objective (UPLAPO 60 $\times$  W, 1.2 N.A., Olympus Europa, Hamburg, Germany). Before entering the objective, the light beam is passed through a Nomarski prism (U-DICTHC, Olympus Europa, Hamburg, Germany) that is normally exploited for differential interference contrast (DIC) microscopy. The principal axes of the Nomarski prism are aligned with the orthogonal polarizations of the laser pulses, so that the prism deflects the laser pulses into two different directions according to their corresponding polarization. After focusing the light through the objective, two overlapping excitation foci are generated, with a small lateral shift between them. The distance between the beams is uniquely defined by the chosen DIC prism and is in our system equal to 403 nm (see Results).

Fluorescence is collected by the same objective (epi-fluorescence setup), passed through the DIC prism and the dichroic mirror, and focused into a single circular aperture (diameter 200  $\mu\text{m}$ ) which is positioned symmetrically with respect to both focus positions and

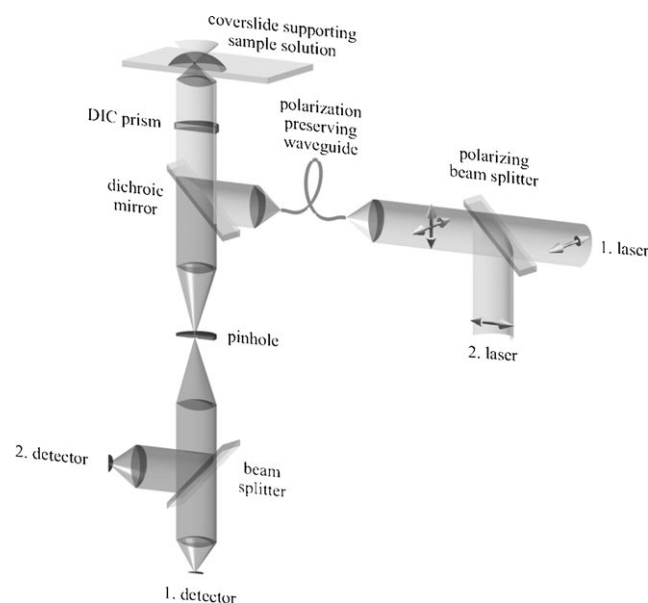


**Figure 1.** Schematic of the 2fFCS setup. Excitation is done by two interleaved pulsed lasers of the same wavelength. The polarization of each laser is linear but orthogonal to each other. Light is then combined by a polarizing beam splitter and coupled into a polarization maintaining optical single-mode fiber. After exiting the fiber, the laser light is collimated by an appropriate lens and reflected by a dichroic beam splitter through a DIC prism. The DIC-prism separates the laser light into two beams according to the polarization of the incoming laser pulses. The microscope objective focuses the two beams into two laterally shifted foci. Fluorescence is collected by the same objective. The tube lens focuses the detected fluorescence from both excitation foci on a single pinhole. Subsequently, the fluorescence light is split by a 50/50 beam splitter and detected by two single photon avalanche diodes (SPADs).

chosen large enough to let the light pass from both foci. Magnification of imaging onto the confocal aperture was  $58\times$ , using a tube lens of 175 mm focal length. After the pinhole, the light is collimated, split by a non-polarizing beam splitter cube (Linus Photonics GmbH & Co. KG, Göttingen, Germany), and focused onto two single-photon avalanche diodes (SPADs, SPCM-AQR-14, Perkin-Elmer, Wellesley, MA, USA). Photon correlation was calculated only between photons of different SPADs for preventing any deterioration of the ACF due to SPAD afterpulsing, see for example, ref. [47]. A dedicated single-photon counting electronics (PicoHarp 200, PicoQuant, Berlin, Germany) is used to record the detected photons. The electronics operates in time-tagged time-resolved (TTTR) mode,<sup>[45]</sup> recording for every detected photon its macroscopic arrival time with 100 ns temporal resolution, and its arrival time with respect to the last laser pulse with picosecond temporal resolution (time-correlated single photon counting, TCSPC<sup>[48]</sup>).

The TCSPC times of each recorded photon are used to decide which laser has excited which fluorescence photon, that is, in which laser focus/detection volume the light was generated. A typical TCSPC histogram measured on an aqueous solution of Atto655 is shown in Figure 2. One can see two different fluorescence decay curves that correspond to the two alternatively pulsing lasers. Atto655 (fluorescence lifetime of ca. 2 ns) was used for all measurements presented in this paper. Pulse distance between laser pulses was 25 ns so that the total probability of detecting a photon from a previous pulse after the next one is  $e^{-12.5} \approx 4 \times 10^{-6}$ , and the chance of associating a detected photon with the wrong laser focus is negligibly small. For fluorescent dyes with significantly

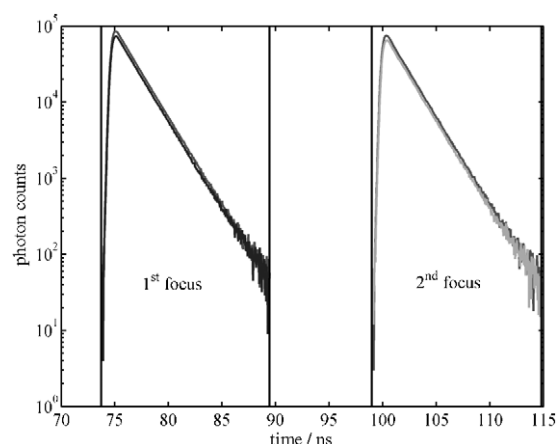


**Figure 2.** TCSPC histograms measured on an aqueous solution of Atto655. The photon counts in the left time window ( $73 \text{ ns} \leq t \leq 89 \text{ ns}$ ) are generated by the first laser that is, first focus, the photon counts in the second time window ( $99 \text{ ns} \leq t \leq 115 \text{ ns}$ ) are generated by the second laser that is, second focus. In both time windows (limited by gray lines in the figure), there are two curves corresponding to the two SPAD detectors, respectively.

longer lifetime, one has to use a sufficiently lower repetition rate for preventing bleed-through between the two time windows. Knowing which photon was generated in which detection volume, autocorrelations for each detection volume as well as cross correlation functions between the two detection volumes are calculated by custom-written software on a PC using MATLAB.<sup>[49]</sup>

Sample temperature was controlled by using a custom-build brass sample holder that was kept at a constant temperature by circulating water through channels in the brass holder. Water temperature was kept at the desired value with a thermostat (F12+MB, JULABO Labortechnik GmbH, Seelbach, Germany). Throughout all 2fFCS experiments, sample temperature was kept at 25 °C.

For PSF scanning, fluorescent beads (PS-Speck Microscope Point Source Kit (P7220), Invitrogen GmbH, Karlsruhe, Germany) were immobilized on a coverslide and scanned through the detection region of the 2fFCS system using a piezo scan table (PI P-527.2CL, Physik Instrumente, Göttingen, Germany) for moving the sample horizontally (with step size of 50 nm), and a piezo actuator (PIFOC P-721-20, Physik Instrumente, Göttingen, Germany) for moving the objective vertically.

A crucial experimental parameter when working with water immersion objectives is correct adjustment of the objective's correction collar to the actual thickness of the used coverslide. Even small deviations between adjusted and actual thickness can have profound effects on the resulting MDF.<sup>[18]</sup> We used the method proposed in ref. [50] for setting the objective's adjustment collar correctly.

**Theory and Data Analysis:** Consider a FCS measurement with two identical but laterally shifted detection regions. Without restriction of generality, let us assume that the shift is along the  $x$ -axis perpendicular to the optical axis of the microscope. Then, the diffusion-determined part of the fluorescence cross-correlation between both detection volumes is given by Equation (1)

$g(t, \delta) =$

$$g_{\infty}(\delta) + \varepsilon_1 \varepsilon_2 c \int dr_1 \int dr_2 U(r_2) \frac{1}{(4\pi Dt)^{3/2}} \exp \left[ -\frac{(r_2 - r_1 - \hat{x}\delta)^2}{4Dt} \right] U(r_1) \quad (1)$$

where  $U(r)$  is the molecule detection function (MDF) giving the position dependent probability to detect a fluorescence photon from a molecule at position  $r$  in one detection volume,  $D$  is the diffusion coefficient,  $c$  the concentration of the molecules, and  $\varepsilon_{1,2}$  are two factors describing the overall excitation power and detection efficiency in both detection volumes, respectively. The vector  $\hat{x}$  is the unit vector along  $x$ , and  $\delta$  is the lateral shift value. For the sake of completeness, we also give here the explicit form of the constant offset  $g_{\infty}(\delta\hat{x})$  of the correlation function shown in Equation (2)

$$g_{\infty}(\delta) = \left[ I_{bg} + \varepsilon_1 c \int dr U(r) \right] \left[ I_{bg} + \varepsilon_2 c \int dr U(r) \right], \quad (2)$$

where  $I_{bg}$  is the background intensity which is, for the sake of simplicity, assumed to be equal for both detection volumes (generalization to non-equal background intensities is straightforward). When setting  $\delta=0$  in Equations (1) and (2) and replacing  $\varepsilon_1 \varepsilon_2$  by either  $\varepsilon_1^2$  or  $\varepsilon_2^2$  one yields the ACF for the separate detection volumes, respectively.

A crucial point for further considerations is to find a sufficiently appropriate model function for the MDF. As it occurs (see Results), a suitable expression is given by Equation (3)

$$U(r) = \frac{\kappa(z)}{w^2(z)} \exp \left[ -\frac{2}{w^2(z)} (x^2 + y^2) \right]. \quad (3)$$

Thus, in each plane perpendicular to the optical axis, the MDF is approximated by a Gaussian distribution having width  $w(z)$  and amplitude  $\kappa(z)/w^2(z)$ . This leads to the explicit cross-correlation function shown in Equation (4)

$$g(t, \delta) = g_{\infty}(\delta) + \frac{\varepsilon_1 \varepsilon_2 c}{4} \sqrt{\frac{\pi}{Dt}} \int_{-\infty}^{\infty} dz_1 \int_{-\infty}^{\infty} dz_2 \frac{\kappa(z_1)\kappa(z_2)}{8Dt + w^2(z_1) + w^2(z_2)} \times \exp \left[ -\frac{(z_2 - z_1)^2}{4Dt} - \frac{2\delta^2}{8Dt + w^2(z_1) + w^2(z_2)} \right]. \quad (4)$$

Before one can use this equation for data fitting, one has to specify  $\kappa(z)$  and  $w(z)$ . As is seen below, an excellent approximation of  $w(z)$  and  $\kappa(z)$  is given by Equation (5)

$$w(z) = w_0 \left[ 1 + \left( \frac{\lambda_{ex} z}{\pi w_0^2 n} \right)^2 \right]^{1/2} \quad (5)$$

and by Equation (6)

$$\kappa(z) = 2 \int_0^z \frac{d\rho\rho}{R^2(z)} \exp \left( -\frac{2\rho^2}{R^2(z)} \right) = 1 - \exp \left( -\frac{2a^2}{R^2(z)} \right), \quad (6)$$

where the function  $R(z)$  shown in Equation (7) is defined by an expression similar to Equation (5):

$$R(z) = R_0 \left[ 1 + \left( \frac{\lambda_{em} z}{\pi R_0^2 n} \right)^2 \right]^{1/2}. \quad (7)$$

In the above equations,  $\lambda_{ex}$  is the excitation wavelength, and  $\lambda_{em}$  the center emission wavelength,  $n$  is the refractive index of the immersion medium (water),  $a$  is the radius of the confocal aperture divided by magnification, and  $w_0$  and  $R_0$  are two (generally unknown) model parameters. Equation (5) simply represents the scalar approximation for the radius of a diverging laser beam with beam waist radius  $w_0$  (see for example, ref. [51]), and Equation (6) is inspired by the work of Qian and Elson<sup>[52]</sup> and Rigler et al.<sup>[14]</sup> concerning the point spread function of confocal imaging. It should be noted that, although Equation (3) looks like the often used Gauss-Lorentz profile, it is *not* such a profile due to the presence of the non-trivial amplitude function  $\kappa(z)$  given in Equation (6).

When inserting Equations (5) and (6) into Equation (4), the resulting expression can be evaluated only numerically, and for doing that it is convenient to change the variables to those shown in Equation (8)

$$\xi = \frac{z_2 - z_1}{2\sqrt{Dt}}, \quad \eta = \frac{z_2 + z_1}{2} \quad (8)$$

leading to the expression in Equation (9)

$$g(t, \delta) = g_{\infty}(\delta) + 2\varepsilon_1 \varepsilon_2 c \sqrt{\pi} \int_0^{\infty} d\xi \int_0^{\infty} d\eta \frac{\kappa(\eta - \sqrt{Dt}\xi)\kappa(\eta + \sqrt{Dt}\xi)}{8Dt + w^2(\eta - \sqrt{Dt}\xi) + w^2(\eta + \sqrt{Dt}\xi)} \times \exp \left[ -\xi^2 - \frac{2\delta^2}{8Dt + w^2(\eta - \sqrt{Dt}\xi) + w^2(\eta + \sqrt{Dt}\xi)} \right] \quad (9)$$

Because  $w$  and  $\kappa$  are rapidly decaying functions for large argument, the infinite integrations over  $\eta$  and  $\xi$  can be approximated by numerically evaluating the integrals within a finite two-dimensional strip defined by  $|\eta \pm \sqrt{Dt}\xi| < M$ , where  $M$  is a truncation value chosen in such a way that the numerical integration result does not change when increasing  $M$  further. Numerical integration is done by using a simple finite element scheme. Convergence is checked by testing whether the numerical result remains the same upon refining the finite element size and when increasing the threshold value  $M$ .

The above equations are becoming slightly more complex when the laser focus is not described by a circular but an elliptic Gaussian distribution (which is always the case when focusing a linearly polarized beam). Assuming that the principal axes of the laser beams are parallel to the  $x$ - and  $y$ -axes, and denoting now the smallest beam waist radii along the principal axes with  $w_{0,1}$  and  $w_{0,2}$ , one has now two functions  $w_1(z)$  and  $w_2(z)$  describing the laser profile, and  $w^2(z)$  in Equation (4) has to be replaced by  $[w_1^2(z) + w_2^2(z)]/2$ . To keep things simple and not to increase the number of independent parameters, we will assume that the effective radius  $\sqrt{[w_1^2(z) + w_2^2(z)]/2}$  is still sufficiently well described by the right hand side of Equation (5) with a single parameter  $w_0$ .

Data fitting is performed with least-square fitting of the model curve, Equation (9), against the measured ACF ( $\delta=0$ ,  $\varepsilon_1 \varepsilon_2$  replaced by either  $\varepsilon_1^2$  or  $\varepsilon_2^2$ ) and cross-correlation CCF *simultaneously* in a global fit. As fit parameters one has  $\varepsilon_1 \sqrt{c}$ ,  $\varepsilon_2 \sqrt{c}$ ,  $D$ ,  $w_0$  and  $R_0$ , as well as three offset values  $g_{\infty}$ . The distance  $\delta$  between the detection regions is determined by the properties of the Nomarski prism and has to be exactly known a priori, thus introducing an external length scale into data evaluation. It is important to notice that a crucial criterion of fit quality is not only to simultaneously repro-

duce the temporal shape of both ACFs and the cross-correlation function, but also to reproduce their three amplitudes  $g_{t \rightarrow 0} - g_{\infty}$  using only the two parameters  $\varepsilon_1 \sqrt{c}$  and  $\varepsilon_2 \sqrt{c}$ . The relation between the amplitudes of the cross-correlation function and the amplitudes of the ACFs is determined by the overlap between the two MDFs, and thus by the shape parameters  $w_0$  and  $R_0$ . Thus, achieving good fit quality for the relative amplitudes of ACF and cross-correlation strongly helps to find the correct values of these parameters. Typical fitting time on a standard Pentium PC takes ca. 1 min using a custom written Matlab routine.

## 2. Results and Discussion

### 2.1 Characterization of the PSF

The MDF model, that is, Equations (3),(5)–(7), was checked by measuring the PSF of the built 2fFCS setup. Immobilized fluorescent beads were scanned at different vertical positions of the objective, choosing a distance of 0.5  $\mu\text{m}$  between adjacent scan planes. Each scan consisted of  $200 \times 200$  pixels<sup>2</sup> of  $50 \times 50$  nm<sup>2</sup> size. Total excitation power was below 1  $\mu\text{W}$  per focus. Using PIE, separate fluorescence images for each laser were reconstructed simultaneously for each scan. A typical scan result is displayed in Figure 3, showing the measured fluorescence intensity distributions in the plane of the beam waist of the focused lasers.

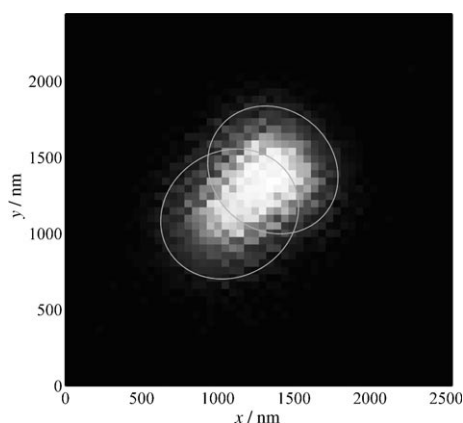


**Figure 3.** Fluorescence intensity scan of a fluorescent bead. The scan plane is the plane of laser beam waist. Solid line shows the  $1/e^2$ -contour of the Gaussian distributions fitted to both laser foci separately. Notice the ellipticity of the laser foci, which are the result of focusing linearly polarized lasers with an objective of high numerical aperture. The  $1/e^2$ -half axes of the foci are 425 nm and 455 nm for the first focus (top right) and 425 nm and 465 nm for the second focus (left bottom). Because both lasers are polarized orthogonal to each other, elongation of both foci is also orthogonal to each other. Laser polarization as well as principal axes of the Nomarski prism are parallel to the image diagonals.

The recorded fluorescence intensity distribution in each plane was fitted by a two-dimensional Gaussian distribution, thus obtaining values of the functions  $w_{1,2}(z)$  and  $\kappa(z)$  at the various  $z$ -positions of the objective. The result for the effective radius  $\sqrt{[w_1^2(z) + w_2^2(z)]/2}$  for both detection regions is

shown in Figure 4, together with a fit using Equation (5). Figure 5 shows the determined values of  $\kappa(z)$  together with a fit using Equations (6) and (7).

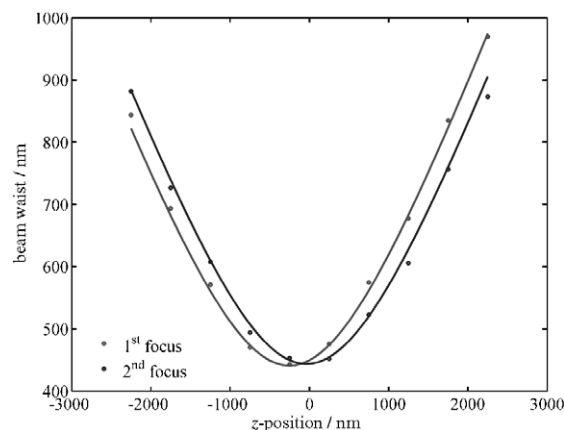


**Figure 4.** Dependence of the effective beam radius of the two PSFs on vertical scan position. Solid lines are fits of Equation (5) to the measured values (circles). Fitted effective beam radius is 440 nm for the first and 445 nm for the second focus.

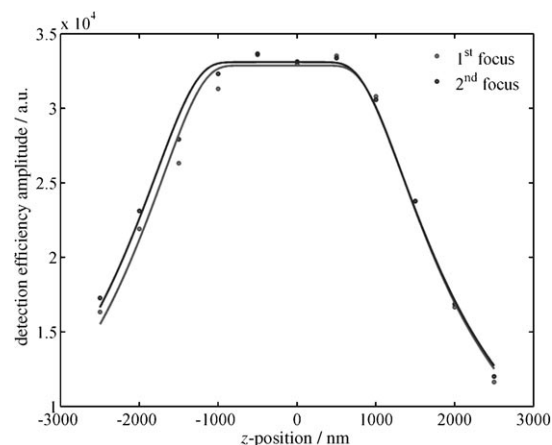


**Figure 5.** Dependence of the amplitude factor  $\kappa(z)$  of the two PSFs on vertical scan position. Solid lines are fits of Equations (6) and (7) to the measured values (circles). Fitted value of  $R_0$  is 130 nm for both foci.

As can be seen from both Figures 4 and 5, the empirical two-parameter model of the MDF fits the measured PSF amazingly well. It should be emphasized that this is far from trivial; for example, Equation (5) fixes the relation between minimum width  $w_0$  of the MDF and its divergence and is inspired by the scalar approximation of the intensity profile of a focused laser beam. However, there is no a priori reason why Equation (5) should be an excellent description of the  $z$ -dependence of the Gaussian width of the MDF, taking into account that 1) laser focusing is done with a high-N.A. objective when one could expect increasing deviation from a scalar beam approximation due to strong non-paraxiality of focusing in connection with the vector character of the electromagnetic field, and that 2) the MDF is not only defined by the laser intensity distribution, but also by the confocal detection. We will present else-

where a detailed wave-optical analysis of the 2fFCS setup, which shows that the simple two-parameter model of the MDF is indeed an excellent approximation. As is also seen, the two-parameter model of the MDF yields excellent fit quality when evaluating measured ACF data.

We repeated PSF scans several times with different beads and determined the lateral shift between the two detection volumes as the distance between the centers of the fitted Gaussian distributions in the plane of the beam waist. We found the value of  $\delta$  to be equal to  $400 \pm 40$  nm. The large variation of this value has several origins. One of them is the inaccuracy of the stepping of the piezo-table which showed non-systematic step-size variations of up to 10%, as was checked by direct imaging of the piezo-table movement using a transparent grid structure with known grid periodicity. Another origin was the limited signal-to-noise ratio and resulting inaccuracy of the Gaussian distribution fits. Also, potential bleaching of the fluorescent dyes during scanning could lead to slight distortions of the measured intensity distributions and thus incorrect determined interfocal distances.

Because the knowledge of the exact focus distance is crucial for a quantitatively precise determination of the diffusion coefficient (its value scales with the square of the adopted focus distance), we adopted another method for determining the focus distance.

## 2.2 Determination of Distance between Foci by z-Scan 2fFCS

When considering FCS measurements in planar two-dimensional systems, there exists one method yielding absolute values of diffusion coefficients without a priori knowledge of the exact PSF of the confocal system, namely the z-scan technique developed by Martin Hof and his group.<sup>[53,54]</sup> The method is based on the validity of Equation (5), that is, on a stringent correlation between divergence and waist of the PSF. We have verified the accuracy of this assumption by direct wave-optical calculations similar to those presented in ref. [18] as well as by scanning the PSF as was shown in the preceding section (see Figure 4). The z-scan technique is then simple and straightforward; one measures ACFs of diffusing molecules within a planar lipid membrane for different vertical positions of the membrane with respect to the focal plane. For the two-dimensional diffusion, the ACF is proportional to  $(1 + 4Dt/w^2)^{-1}$ , where  $w$  is the width of the Gaussian profile of the PSF within the plane of diffusion. Next, one fits the measured ACFs with this expression and plots  $w^2/4Dt$  as a function of vertical position  $z$ . Knowing that  $w(z)$  has to obey Equation (5), the diffusion coefficient  $D$  and the beam waist  $w_0$  are obtained separately and in absolute numbers. On the other hand, using 2fFCS and knowing the exact distance  $\delta$  between the laser foci, one can obtain the values of  $w$  and  $D$  already from one measurement by using the relation in Equation (10)<sup>[30]</sup>

$$g(t, \delta) = g_{\infty}(\delta) + \frac{\varepsilon^2 c}{4\pi D t w^4} \int \int d\rho_2 d\rho_1 \exp\left(-\frac{2\rho_2^2}{w^2} - \frac{2\rho_1^2}{w^2} - \frac{|\rho_2 - \rho_1 + \delta|^2}{4Dt}\right) = g_{\infty}(\delta) + \frac{\pi \varepsilon^2 c}{4} \frac{1}{4Dt + w^2} \exp\left(-\frac{\delta^2}{4Dt + w^2}\right) \quad (10)$$

which is valid for purely two-dimensional diffusion through to molecule detection functions described by two-dimensional Gaussians with diameter  $w$  and a distance  $\delta$  apart. Similar to the Theory and Data Analysis section,  $\varepsilon$  is a parameter describing the overall excitation power times detection efficiency, and  $c$  is the molecule concentration per area. For obtaining the value of  $\delta$ , we performed 2fFCS measurements on lipid diffusion within the lipid bilayer of a giant unilamellar vesicle (GUV) for different z-positions and used Equation (10) to obtain  $w$  as a function of  $z$ . A typical 2fFCS measurement is shown in Figure 6, together with a theoretical fit. The correct value of  $\delta$

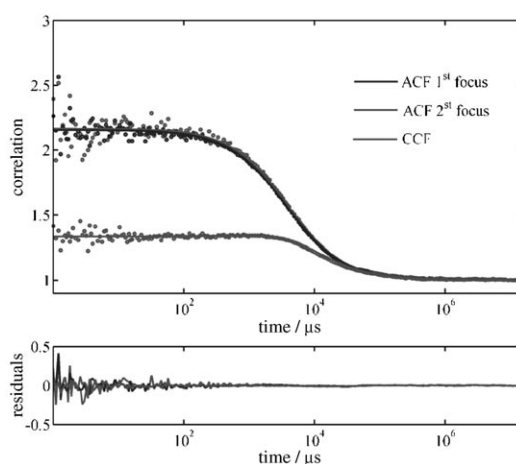


**Figure 6.** 2fFCS measurement of lipid diffusion in a GUV. Lipids were sparsely labelled with Atto655. Shown are the autocorrelation functions for the first focus (ACF 1st focus), second focus (ACF 1st focus), and the cross-correlation between both foci (CCF). Total cw-excitation power per laser was 2  $\mu$ W, measurement time was 10 min. Circles are experimental values, solid lines are global fits using Equation (10).

was found by the dependence of  $w$  on  $z$  from Equation (5), that is, that the one-focus z-scan FCS and the 2fFCS yield identical results. The 2fFCS z-scan was performed on the same GUV twice by first moving the focus up and afterwards down, thus checking that there was no mechanical vertical drift of the measurement system. Both z-scans yielded the identical value of 403 nm for  $\delta$ , a value in excellent agreement with the manufacturer's specifications for the used Nomarski prism. It should be noted that we performed the measurements on GUVs instead of using supported lipid bilayers; this prevents any potential artefacts stemming from the interaction between lipids and the support.

It should be also noted that, due to the slight off-center position of the two laser foci with respect to the confocal aperture, the apparent distance between the Gaussian intensity dis-

tributions becomes slightly smaller when moving farther away ( $>2\ \mu\text{m}$ ) from the focal plane. However, in the subsequent 2fFCS data analysis, this slight bending of the MDF is ignored and we used the model MDF as presented in the Theory and Data Analysis section, assuming axial symmetric MDFs with a lateral distance that is independent of the  $z$ -position. We adopted a value of  $\delta = 403\ \text{nm}$  for the 2fFCS data analysis. This parameter is the basic characteristic of the 2fFCS setup fixing the length scale of the diffusion measurement. For a given excitation wavelength, it is completely determined by the optical properties of the used Nomarski prism and does not depend on optical parameters such as coverslide thickness, sample refractive index, laser beam diameter etc. The Nomarski prism generates two *parallel* light beams in the sample, which are identical to laser foci without the prism but shifted perpendicularly to the optical axis.<sup>[55]</sup> Thus, any aberrations caused by stratified media oriented perpendicular to optical axis will deform the focused light intensity distribution but does not change the distance between the axes of propagation of both foci.<sup>[56,57]</sup> A similar optical argument applies also for the detection, see refs. [55,58,59]. The determined diffusion coefficient of a 2fFCS measurement scales with the square of the inter-focal distance. Thus, for achieving absolute accuracy of better than 4% in diffusion measurements, this value has to be known with accuracy better than 2% or better than 8 nm in our case. In practice, the best way to determine its precise value is to perform a 2fFCS measurement on a reference sample with precisely known diffusion, which is much simpler than performing a full  $z$ -scan on a GUV.

### 2.3 Viscosity-Dependent Diffusion and Refractive Index Mismatch

We measured ACFs for solutions of Atto655 in aqueous solutions of guanidine hydrochloride (GdHCl) at different GdHCl concentrations. Atto655 has the particular property that it does not show any discernable triplet state dynamics when dissolved in water, which makes it an ideal dye for checking FCS-based diffusion measurements. Both the refractive index and the viscosity of GdHCl solutions are strongly changing with increasing GdHCl concentration.<sup>[60]</sup> Each measurement lasted for 10 min, and for each GdHCl concentration measurements were repeated ten times to determine a standard deviation for the diffusion coefficient. A typical measurement on an aqueous solution of Atto655 is shown in Figure 7, together with a global fit of all three curves using Equation (9). As can be seen, the obtained fit quality is excellent. The determined values of the diffusion coefficient for all measured solutions of GdHCl are shown in Figure 8 as a function of the inverse value of viscosity. Solution viscosity was determined using the known dependency of viscosity on GdHCl concentration.<sup>[60]</sup> For checking the validity of the 2fFCS results, diffusion of Atto655 was measured in deuterized methanol using pulse-field gradient NMR. The corresponding value is also shown in Figure 8. Assuming that the diffusion coefficient is strictly proportional to the inverse of the viscosity and independent of the chemical nature of the solvent (GdHCl in water, deuterized methanol), a linear least-square fit was applied to all GdHCl values of the diffusion coefficient and is also displayed in Figure 8. The results demonstrate 1) that there is fair agreement between the diffusion coefficient as determined by pulse-field gradient NMR and the absolute values obtained with 2fFCS and 2) that the 2fFCS measurements at different GdHCl concentrations excellently reproduce the expected linear dependence of diffusion coefficient on the inverse value of viscosity, thus demonstrating that 2fFCS works well even for large mismatch between sample refractive index and the refractive index of the objective's immersion medium (pure water).

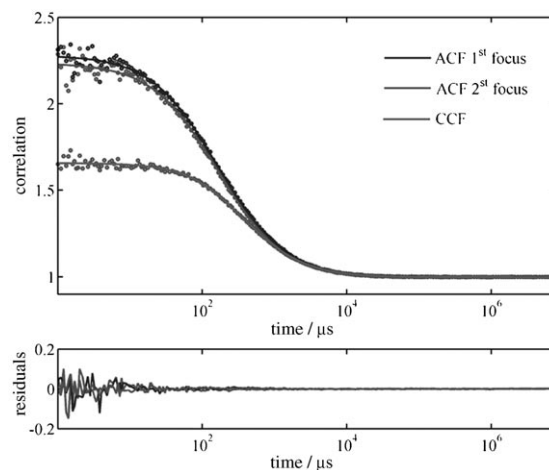


**Figure 7.** 2fFCS measurement on a nanomolar aqueous solution of Atto655 (cw-excitation power per laser:  $20\ \mu\text{W}$ , measurement time: 1 hour). As before, the autocorrelation functions for the first focus (ACF 1st focus), second focus (ACF 2nd focus), and the cross-correlation between both foci (CCF) are shown. The shape of both ACFs is virtually identical. Circles are experimental values, solid lines are global fits using Equation (9).

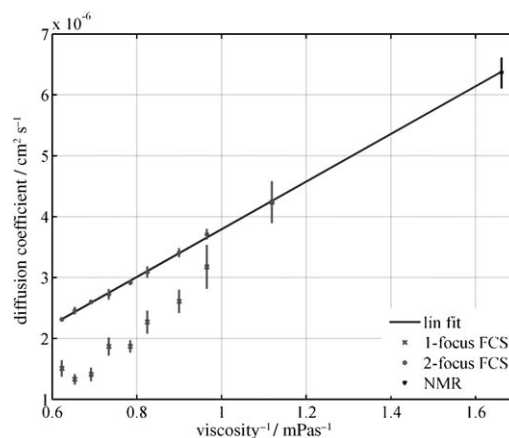


**Figure 8.** Dependence of the diffusion coefficient of Atto655 in aqueous GdHCl solutions (dots) and in  $d_4$ -deuterized methanol (triangle) at  $25\ ^\circ\text{C}$  as a function of solvent viscosity. The solid line represents the linear least square fit to all data. Standard deviations are shown as error bars and are each derived from ten repeated measurements. For comparison, the results of single-focus FCS using a standard model that assumes a three-dimensional Gaussian MDF are also shown (crosses). Because single-focus FCS can only measure relative values of diffusion coefficient, we took the value for pure water as the reference value.

no), a linear least-square fit was applied to all GdHCl values of the diffusion coefficient and is also displayed in Figure 8. The results demonstrate 1) that there is fair agreement between the diffusion coefficient as determined by pulse-field gradient NMR and the absolute values obtained with 2fFCS and 2) that the 2fFCS measurements at different GdHCl concentrations excellently reproduce the expected linear dependence of diffusion coefficient on the inverse value of viscosity, thus demonstrating that 2fFCS works well even for large mismatch between sample refractive index and the refractive index of the objective's immersion medium (pure water).

In absolute numbers the diffusion coefficient of Atto655 in water at 25 °C, determined with 2fFCS, is equal to  $(4.26 \pm 0.08) \times 10^{-6} \text{ cm}^2 \text{ s}^{-1}$ . The NMR value extrapolated to the viscosity of water is  $(4.29 \pm 0.13) \times 10^{-6} \text{ cm}^2 \text{ s}^{-1}$ , which is in excellent agreement with our 2fFCS measurement.

The increasing refractive index mismatch with increasing GdHCl concentration leads to increasingly larger fit values of  $w_0$  and  $R_0$  as shown in Figure 9. This reflects the increasingly

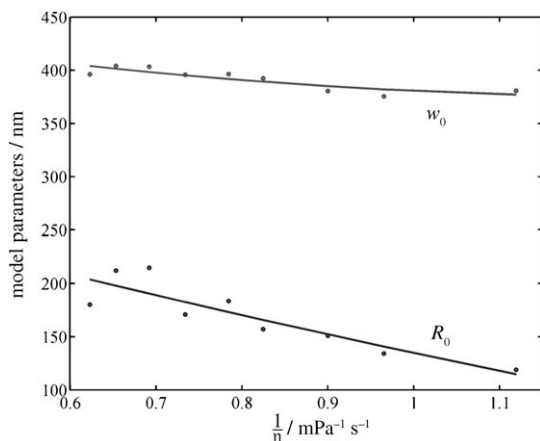


**Figure 9.** Dependence of the fitted values of  $w_0$  and  $R_0$  on inverse viscosity (for better comparison with Figure 8). Shown are experimental values (circles) and second order polynomial fits (solid lines). Both values increase with increasing viscosity and thus refractive index of the solution, reflecting a MDF changed by aberrations that are induced by refractive-index mismatch.

larger detection volume due to increasingly larger mismatch-induced optical aberrations. However, the used two-parameter model for the MDF is obviously flexible enough to approximate the shape of the distorted detection volumes well enough so that one still obtains correct values for the diffusion coefficient. This is an important feature of 2fFCS, making it an ideal tool to monitor for example, hydrodynamic radii of proteins during chemical unfolding in GdHCl solutions.<sup>[61]</sup> It should be mentioned that the insensitivity of 2fFCS with respect to refractive index mismatch also implies its insensitiveness with respect to cover slide thickness variations, because these variations introduce quite similar spherical aberrations as the refractive index mismatch.

## 2.4 Excitation Intensity Dependence

An important source of inaccuracy in standard FCS measurements is the dependence of the measured diffusion time on excitation intensity due to optical saturation of fluorescence. Because the fluorescence properties of many fluorescing dyes used for labelling proteins, DNA or RNA are changing upon binding to the labelled molecules (most often due to changes in intersystem crossing rate), and thus their optical saturation behavior, even comparative measurements of diffusion coefficients with the free dye as reference are problematic. Even worse, as was shown both experimentally<sup>[21]</sup> and theoretically,<sup>[18]</sup> the change of apparent diffusion coefficient with increas-

ing excitation intensity is largest in the limit of infinitely small intensity, making even an extrapolation of measured values toward zero excitation intensity difficult and imprecise. To check the robustness of 2fFCS against changes in excitation intensity, we performed measurements on aqueous solutions of Atto655 at different total excitation powers (per laser) between 10 and 70  $\mu\text{W}$ . The resulting dependence of determined diffusion coefficient on excitation intensity is displayed in Figure 10.

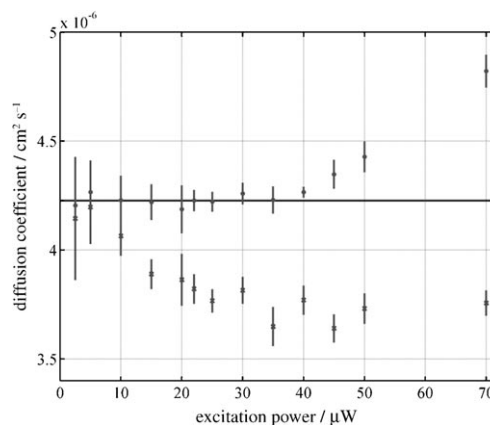


**Figure 10.** Dependence of the measured diffusion coefficient of Atto655 in aqueous solution at 25 °C as a function of excitation power per laser (dots). Solid line is the value of the diffusion coefficient for pure water as derived from the measurements shown in Figure 7. Again, the results of single-focus FCS are also shown (crosses). As reference value we extrapolated the single-focus FCS results towards zero intensity, assuming this value to be equal to the value as measured by 2fFCS (solid horizontal line).

As can be seen, there is virtually no dependence of the determined diffusion coefficient on excitation intensity up to an excitation power of ca. 40  $\mu\text{W}$ . We interpret the subsequent rise in apparent diffusion coefficient as caused by the increasing impact of photobleaching. That the diffusion coefficient measured with 2fFCS remains constant over a large range of excitation intensities is in stark contrast to that observed in standard FCS, where a prominent decrease of the apparent diffusion coefficient (i.e. increase in observed diffusion times) for increasing excitation intensities (as long as this is not counterweighted by increasing photobleaching at large intensities) is observed. Figure 11 presents the change in fitted values of  $w_0$  and  $R_0$  with increasing excitation intensity. Similar to the case of refractive index mismatch (see previous section), the value of  $w_0$  increases with increasing excitation intensity and thus optical saturation, whereas the value of  $R_0$  changes only slightly. This shows again that the simple two-parameter model of the MDF is flexible enough to accommodate to aberrations, but that the aberrations introduced by refractive index mismatch and by optical saturation are clearly different.

Finally, it should be noted that our method (and, as far as we know, no other FCS method) is not capable of compensating or correctly dealing with photobleaching. Photobleaching is an irreversible photo-destruction of fluorescent molecules in solution, leading to a *time-dependent* inhomogeneous concentration profile and thus invalidating the fundamental assump-

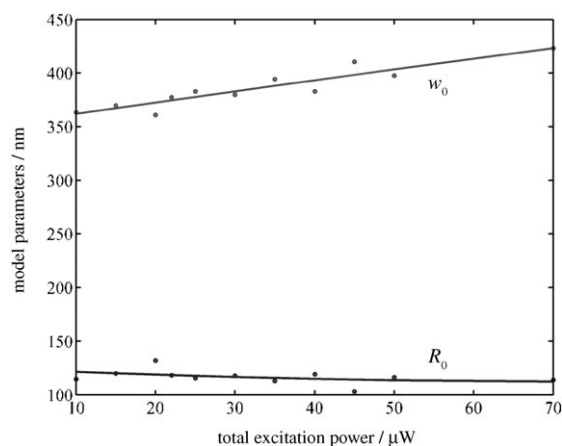


**Figure 11.** Dependence of the fitted values of  $w_0$  and  $R_0$  on excitation power. Shown are experimental values (circles) and second order polynomial fits (solid lines). Here, the value of  $w_0$  changes most with increasing aberrations induced by optical saturation, whereas  $R_0$  remains rather unchanged.

tion of all FCS analysis, namely the measurement is stationary (measurement should be invariant with respect to time shift). Thus, one has always to check that the used excitation intensity is below the threshold where any photobleaching effects are detected.

### 3. Discussion and Conclusion

We have presented a new method to measure diffusion coefficients at the infinite dilution limit based on a standard confocal FCS setup. In contrast to standard FCS, not only was an external ruler introduced, but also a new two parameter model describing the MDF was invented, which is used to evaluate the recorded data. The two parameter model has proven to fit recorded MDFs perfectly. Even with optical aberrations present, the model still approximates the MDF good enough to deliver the correct diffusion values. This is by far a non-trivial fact. Although these aberrations will certainly deform the MDF of each focus (in an identical way), the distance *between* both detection regions is not changed by aberrations caused by coverslide thickness deviation or refractive index mismatch, or optical saturation. And indeed, we obtain different values for the fit parameters  $w_0$  and  $R_0$  for different excitation power or different sample refractive index values, reflecting the changes of the MDF with increasing aberration. However, the final result for the diffusion coefficient is still remarkably correct although the “ideal” MDF model function as described by Equations (3)–(7) will certainly no longer be exact. Extended wave-optical modeling of 2fFCS experiments that confirm this empirical finding will be presented elsewhere, and are far beyond the scope of the current paper.

We show that 2fFCS is robust against refractive index changes of the sample medium (and, indirectly, against coverslide thickness variations) and optical saturation. These properties and the high measurement accuracy make 2fFCS an ideal tool to study protein folding/unfolding where other methods

fail due to sample aggregation or photophysical/optical artefacts.

To our knowledge, we publish the first absolutely determined diffusion coefficient of a red fluorescent dye (Atto655). This value can serve as a reference for calibrating standard FCS setups in the red spectral region.

### Acknowledgements

We are deeply indebted to the generous support of our work by the whole team of PicoQuant Company (Berlin), especially to Felix Koberling and Rainer Erdmann. Financial support by the Deutsche Volkswagenstiftung, the Deutsche Forschungsgemeinschaft, and the Forschungszentrum Jülich is gratefully acknowledged.

**Keywords:** diffusion coefficients · fluorescence spectroscopy · fluorescent dyes · time-resolved spectroscopy

- [1] A. Einstein, *Investigations on the Theory of the Brownian Movement*, Dover, New York, **1985**.
- [2] A. M. Weljie, A. P. Yamniuk, H. Yoshino, Y. Izumi, H. J. Vogel, *Protein Sci.* **2003**, *12*, 228–236.
- [3] B. J. Berne, R. Pecora, *Dynamic Light Scattering*, Dover, New York, **2000**.
- [4] P. T. Callaghan, *Principles of Nuclear Magnetic Resonance Microscopy*, Clarendon, Oxford, **1991**.
- [5] D. Harvey, *Modern Analytical Chemistry*, McGraw-Hill, Boston, **2000**, pp. 593–595.
- [6] J. L. Cole, J. C. Hansen, *J. Biomol. Tech.* **1999**, *10*, 163–176.
- [7] W. Liu, T. Cellmer, D. Keerl, J. M. Prausnitz, H. W. Blanch, *Biotechnol. Bioeng.* **2005**, *90*, 482–490.
- [8] T. Kiefhaber, R. Rudolph, H. H. Kohler, J. Buchner, *Nat. Biotechnol.* **1991**, *9*, 825–829.
- [9] D. Magde, E. Elson, W. W. Webb, *Phys. Rev. Lett.* **1972**, *29*, 705–708.
- [10] E. L. Elson, D. Magde, *Biopolymers* **1974**, *13*, 1–27.
- [11] D. Magde, E. Elson, W. W. Webb, *Biopolymers* **1974**, *13*, 29–61.
- [12] J. Widengren, Ü. Mets in *Single-Molecule Detection in Solution—Methods and Applications* (Eds.: C. Zander, J. Enderlein, R. A. Keller), Wiley-VCH, Weinheim, **2002**, pp. 69–95.
- [13] *Fluorescence Correlation Spectroscopy* (Eds.: R. Rigler, E. Elson), Springer, Berlin, **2001**.
- [14] R. Rigler, Ü. Mets, J. Widengren, P. Kask, *Eur. Biophys. J.* **1993**, *22*, 169–175.
- [15] S. T. Hess, W. W. Webb, *Biophys. J.* **2002**, *83*, 2300–2317.
- [16] T. D. Perroud, B. Huang, M. I. Wallace, R. N. Zare, *ChemPhysChem* **2003**, *4*, 1121–1123.
- [17] J. Enderlein, I. Gregor, D. Patra, J. Fitter, *Curr. Pharm. Biotechnol.* **2004**, *5*, 155–161.
- [18] J. Enderlein, I. Gregor, D. Patra, T. Dertinger, B. Kaupp, *ChemPhysChem* **2005**, *6*, 2324–2336.
- [19] K. Berland, G. Shen, *Appl. Opt.* **2003**, *42*, 5566–5576.
- [20] G. Nishimura, M. Kinjo, *Anal. Chem.* **2004**, *76*, 1963–1970.
- [21] I. Gregor, D. Patra, J. Enderlein, *ChemPhysChem* **2005**, *6*, 164–170.
- [22] H. Rigneault, P. F. Lenne, *J. Opt. Soc. Am. B* **2003**, *20*, 2203–2214.
- [23] S. K. Davis, C. J. Bardeen, *Rev. Sci. Instrum.* **2002**, *73*, 2128–2135.
- [24] R. L. Hansen, J. M. Harris, *Anal. Chem.* **1998**, *70*, 4247–4256.
- [25] R. Jaffiol, Y. Blancquaert, A. Delon, J. Derouard, *Appl. Opt.* **2006**, *45*, 1225–1235.
- [26] J. Enderlein, *Chem. Phys. Lett.* **1999**, *308*, 263–266.
- [27] K. Q. Xia, Y. B. Xin, P. Tong, *J. Opt. Soc. Am. A* **1995**, *12*, 1571–1578.
- [28] M. Brinkmeier, K. Dörre, J. Stephan, M. Eigen, *Anal. Chem.* **1999**, *71*, 609–616.
- [29] P. S. Dittrich, P. Schwille, *Anal. Chem.* **2002**, *74*, 4472–4479.
- [30] J. Ries, P. Schwille, *Biophys. J.* **2006**, *91*, 1915–1924.

- [31] M. I. Angelova, D. S. Dimitrov, *Faraday Discuss. Chem. Soc.* **1986**, *81*, 303–308.
- [32] P.-Y. Bolinger, D. Stamou, H. Vogel, *J. Am. Chem. Soc.* **2004**, *126*, 8594–8595.
- [33] R. F. Karlicek, I. J. Lowe, *J. Magn. Reson.* **1980**, *37*, 75–91.
- [34] A. Chen, C. S. Johnson, Jr., M. Lin, M. J. Shapiro, *J. Am. Chem. Soc.* **1998**, *120*, 9094–9095.
- [35] R. M. Cotts, M. J. R. Hoch, T. Sun, J. T. Marker, *J. Magn. Reson.* **1989**, *83*, 252–266.
- [36] E. J. Fordham, S. J. Gibbs, L. D. Hall, *Magn. Reson. Imaging* **1994**, *12*, 279–284.
- [37] D. Wu, A. Chen, C. S. Johnson, Jr., *J. Magn. Reson. A* **1995**, *115*, 260–264.
- [38] S. J. Gibbs, C. S. Johnson, Jr., *J. Magn. Reson.* **1991**, *93*, 395–402.
- [39] K. F. Morris, C. S. Johnson, Jr., *J. Am. Chem. Soc.* **1992**, *114*, 3139–3141.
- [40] H. Weingärtner, M. Holz, A. Sacco, M. Trotta, *J. Chem. Phys.* **1989**, *91*, 2568–2574.
- [41] M. Holz, H. Weingärtner, *J. Magn. Reson.* **1991**, *92*, 115–125.
- [42] W. Price, *Concepts Magn. Reson.* **1998**, *10*, 197–237.
- [43] C. S. Johnson, Jr., *Prog. Nucl. Magn. Reson. Spectrosc.* **1999**, *34*, 203–256.
- [44] B. Antalek, *Concepts Magn. Reson.* **2002**, *14*, 225–258.
- [45] M. Böhmer, F. Pampaloni, M. Wahl, H. J. Rahn, R. Erdmann, J. Enderlein, *Rev. Sci. Instrum.* **2001**, *72*, 4145–4152.
- [46] B. K. Müller, E. Zaychikov, C. Bräuchle, D. Lamb, *Biophys. J.* **2005**, *89*, 3508–3522.
- [47] J. Enderlein, I. Gregor, *Rev. Sci. Instrum.* **2005**, *76*, 033 102.
- [48] D. V. O'Connor, D. Phillips, *Time-Correlated Single Photon Counting*, Academic Press, London, **1984**.
- [49] M. Wahl, I. Gregor, M. Patting, J. Enderlein, *Opt. Express* **2003**, *11*, 3583–3591.
- [50] M. Schwertner, M. J. Booth, T. Wilson, *J. Microsc.* **2005**, *217*, 184–187.
- [51] J. Enderlein, F. Pampaloni, *J. Opt. Soc. Am. A* **2004**, *21*, 1553–1558.
- [52] H. Qian, E. L. Elson, *Appl. Opt.* **1991**, *30*, 1185–1195.
- [53] A. Benda, M. Benes, V. Marecek, A. Lhotsky, W. T. Hermens, M. Hof, *Langmuir* **2003**, *19*, 4120–4126.
- [54] J. Humpolicková, E. Gielen, A. Benda, V. Fagulova, J. Vercammen, M. VandeVen, M. Hof, M. Ameloot, Y. Engelborghs, *Biophys. J.* **2006**, *91*, L23–L25.
- [55] P. R. T. Munro, P. Török, *Opt. Express* **2005**, *13*, 6833–6847.
- [56] P. Török, Z. Varga, G. R. Laczik, J. Booker, *J. Opt. Soc. Am. A* **1995**, *12*, 325–332.
- [57] P. Török, P. Varga, *Appl. Opt.* **1997**, *36*, 2305–2312.
- [58] O. Haeblerlé, M. Ammar, H. Furukawa, K. Tenjimbayashi, P. Török, *Opt. Express* **2003**, *11*, 2964–2969.
- [59] J. Enderlein, M. Böhmer, *Opt. Lett.* **2003**, *28*, 941–943.
- [60] K. Kawahara, C. Tanford, *J. Biol. Chem.* **1966**, *241*, 3228–3232.
- [61] K. Chattopadhyay, S. Saffarian, E. L. Elson, C. Frieden, *Biophys. J.* **2005**, *88*, 1413–1422.

---

Received: October 13, 2006

Revised: December 10, 2006

Published online on January 31, 2007